POLITECNICO DI TORINO
Repository ISTITUZIONALE

Multistage carrier phase estimation algorithms for phase noise mitigation in 64-quadrature amplitude modulation optical systems

Terms of use:

Publisher copyright

(Article begins on next page)

14 May 2024

Multi-stage CPE algorithms for phase noise mitigation in 64-QAM optical systems

S. M. Bilal, Student Member, IEEE, C. Fludger, V. Curri, Member, IEEE and G. Bosco, Senior Member, IEEE

Abstract—Two novel low-complexity multi-stage digital feed-forward carrier phase estimation (CPE) algorithms for 64-ary quadrature amplitude modulation (QAM) are proposed and analyzed by numerical simulations. The first stage is composed of a Viterbi&Viterbi block, based on either the standard quadrature phase shift keying (QPSK) partitioning algorithm using only Class-1 symbols or a modified QPSK partitioning scheme utilizing both Class-1 and outer most triangle-edge (TE) symbols. The second stage applies the Viterbi&Viterbi algorithm after a 64-QAM-to-QPSK transformation, while the subsequent stages iterate a maximum likelihood estimation (MLE) algorithm for phase estimation. All proposed techniques are characterized by a high tolerance to laser phase noise: an OSNR penalty of 1 dB at bit error rate (BER) of 10^{-2}, the proposed schemes can tolerate a linewidth times symbol duration product ($\Delta\nu \cdot T_s$) equal to 5.6×10^{-5} and 7.1×10^{-5}, respectively. At 32 Gbaud, all of the above linewidth requirements can be met using commercial tunable lasers. The proposed schemes achieve a similar linewidth tolerance with a reduced implementation complexity with respect to algorithms based on the blind phase search (BPS) method.

Index Terms—Bit error rate (BER), carrier phase recovery, Viterbi & Viterbi algorithm, quadrature amplitude modulation (QAM), maximum likelihood estimation (MLE), triangle edge (TE) symbols, 64-QAM–QPSK transformation

I. INTRODUCTION

Due to its high tolerance towards linear and non-linear fiber impairments and improved spectral efficiency, coherent optical detection combined with polarization multiplexing and multi-level modulation formats has drawn a considerable attention in the past few years. Multilevel M-ary QAM formats are considered to be the best candidate for future high-capacity 100 and 400 Gbps wavelength-division multiplexing (WDM) systems [1]–[5]. However, high-order QAM formats, such as 64-QAM, can be severely affected by the phase noise generated by the finite linewidth of both transmitter (Tx) laser and receiver (Rx) local oscillator [6], [7]. Phase noise results in distortion and hence random rotation of the received constellation points [8]. As a result, the design of improved laser linewidth tolerant carrier phase estimation (CPE) algorithms has become very important for successful implementation of these high-order modulation formats.

Up till now, three main classes of CPE algorithms have been reported in the literature. The first one is based on a decision

S.M. Bilal, V. Curri and G. Bosco are with Dipartimento di Elettronica, Politecnico di Torino, Italy (e-mail: gabriella.bosco@polito.it). C. Flugder is with Cisco Optical GmbH, Nurnberg, Germany (e-mail: cfludge@cisco.com).

directed feedback loop [8]–[10]. Laser linewidth tolerance of this method is not very promising because the estimation of phase depends on the previous set of data symbols instead of the current one, hence making this algorithm complex at the implementation level [11], [12]. The second class is based on a blind phase search (BPS) algorithm. Although this algorithm can attain a high phase noise tolerance, it comes at an expense of a large computational complexity [13]. With the increase in the modulation level, the required number of test phase angles also increases and can be very significant for higher order QAM formats (e.g > 32 is required for square 64QAM [14]). The third class of algorithms is based on the classic feed-forward Viterbi and Viterbi (V&V) M-th power digital phase estimation algorithm [15]. When applied to high-order modulation formats, it requires dedicated symbols and ad-hoc amplitude discrimination for carrier phase estimation [13], [16]. However, V&V algorithms are simpler to implement and have much smaller computational complexity.

In this paper we propose two multi-stage low complexity feed-forward algorithms to compensate for the phase noise in 64-QAM systems. Both algorithms consist of four stages. The first stage is used to perform a coarse phase estimation, which is refined in the second stage by applying a 64-QAM-to-QPSK transformation [17], followed by the standard 4-th power Viterbi&Viterbi algorithm. A further refinement in the estimation can be obtained by iterating a maximum-likelihood estimation (MLE) scheme in the subsequent stages. We also analyze, for the first time to our knowledge, the effect of the cascade of several CPE blocks (implementing a sort of "turbo" carrier phase estimation), finding that some advantage can be obtained up to the fourth iteration, while additional iterations do not give any substantial gain. The remainder of the paper is organized as follows. In Section II, an overview of the conventional CPE technique based on V&V and MLE is given. In Section III, a modification in this scheme to include TE symbols is described while the 64-QAM–QPSK transformation algorithm, that serves as a second stage for both the techniques is explained in Section IV. Section V describes the multi-stage CPE architectures, whose performance is analyzed by simulation in Section VI. Most of the published papers on CPE algorithms [1]–[4], [9]–[16], [18], [19] typically consider reference BER values around 10^{-3} or 10^{-4}. In our study we decided to use 10^{-2} instead of 10^{-3} or 10^{-4} in order to check the performance of the algorithms at a BER threshold closer to the performance of state-of-the-art advanced FECs. Section VII is devoted to final comments and conclusions.
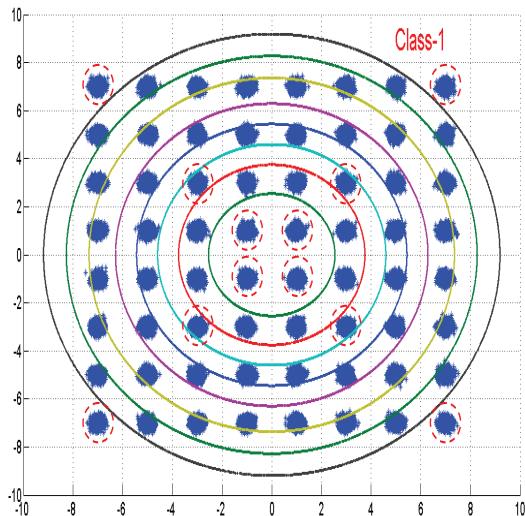
Fig. 1. 64-QAM Constellation with different thresholds for separating symbols of different amplitudes. Class-1 symbols used in the first Viterbi&Viterbi stage are highlighted by red dashed circles.

II. CONVENTIONAL CPE TECHNIQUES OVERVIEW

Fig. 1 shows the constellation plot of a 64-QAM system affected by Additive Gaussian Noise (AGN), as for instance the Amplified Spontaneous Emission (ASE) noise introduced by optical amplifiers. Circles in the figure indicate the different thresholds for separating symbols of different amplitudes. One possible approach is to perform phase estimation using the conventional V&V algorithm considering only Class-1 symbols, i.e. symbols that lie at modulation angles of $\pi/4 + m \cdot \pi/2$ (m=0...3). These symbols are indicated with red dashed circles in Fig. 1. Note that only 12 out of the 16 symbols lying at the vertices of squares are used. The remaining four are neglected since, having a modulus very similar to other constellation points, their identification is critical and would lead to additional errors. The block diagram of the algorithm is shown in Fig. 3a. The complex samples are raised to the 4-th power to remove the phase modulation. To increase the accuracy of the estimate, a moving average with a uniform centered window of length N_1 symbols is performed. By finding the angle of the complex sum vector, a phase error estimate is obtained for this block. The complex samples are normalized before adding them up for phase estimation:

$$\varphi_{est,class1} = \frac{1}{4} arg \sum_{k=1}^{N_1} \frac{X_k^4}{|X_k^4|} \qquad (1)$$

Whenever a symbol is received that does not belong to Class-1, a 'zero' is inserted at its place in the vector of samples used for phase estimation in Eq. (1), .i.e. that particular symbol does not give any contribution to the phase estimation but the length of the averaging window N_1 includes also non-Class-1 symbols.

Since only a small percentage of all the symbols is used ($\approx 19\%$), phase estimation obtained by using these symbols is not suitable to track fast phase variations: it is potentially able to compensate for a laser linewidth which is approximately

1/5 of the linewidth that could be compensated for if all 64 symbols were used.

A further improvement in the performance of this estimator can be obtained by adding one or more Maximum Likelihood Estimation (MLE) stages, whose block diagram is shown in Fig. 3d. While for 16-QAM systems adding more than one MLE stage does not have any significant impact on the phase estimation [18], for a 64-QAM system we observed that there is always some residual phase noise after the 1st MLE stage and the addition of further MLE stages may be beneficial [20]. The ML estimation of the carrier phase is obtained as [13],

$$z = \sum_{k=1}^{N_2} x_k \cdot y_k^* \qquad (2)$$

$$\varphi_{ML} = tan^{-1} \left(\frac{Im(z)}{Re(z)} \right) \qquad (3)$$

where y_k is the decision of x_k and N_2 is the averaging window length for the MLE stage.

III. MODIFIED V&V ALGORITHM (V&V*)

In [18], [21], we have shown that a better phase noise tolerance can be achieved, if it is possible to increase the number of symbols that took part in the phase estimate. This is mainly due to the fact that, for a larger number of points, a lower averaging window length can be used. However, since in [21] the symbols were raised to the power of eight instead of four, cycle slips could occur resulting in phase rotation/de-rotation of the received constellation points by integer multiples of $\pi/4$ (instead of $\pi/2$, as in conventional V&V algorithm). This would generate, after CPE, a rhombus-like constellation in place of the standard square-like constellation. So the technique proposed in [21] worked well for a low BER (around 10^{-3}) but, moving towards higher target BER values, the effect of cycle slips could become detrimental and could cause severe degradation in performance. A possible countermeasure is based on the technique proposed in [22] for cycle slips detection and compensation. Eq. (2) in [22] can be used, by substituting the raising to the power of 2 to a raising to the power of 4.

Another possible approach consists of increasing the number of constellation points used for phase estimation by raising to the power of four not only Class-1 symbols, but also symbols which lie at an angle close but not exactly equal to $\pi/4 + m \cdot \pi/2$ (m=0...3). In this way, the number of symbols that take part in the phase estimate is increased and a better phase noise tolerance is achieved, provided that the angle of deviation of the new symbols with respect to Class-1 symbols is sufficiently small.

Hence for this estimator Class-1 symbols of the inner 16-QAM along with the outermost triangle edge (TE) symbols of the 64-QAM constellation are selected (Fig. 2). In Fig. 2 TE and Class-1 symbols are shown by green dashed triangles and red dashed circles, respectively. The block diagram is shown in Fig. 3b, where, phase estimation is obtained by using conventional VVPE algorithm by raising the symbols to the power of 4 (see eq. (1)). Averaging is performed over N_1

(a) V&V

Incoming Data

↓

Partition Class-1 Symbols

↓

Symbols^4

↓

VVPE (Block Size N1)

$e^{-j\varphi_{est}}$ φ_{est}

⊗

↓

(b) V&V*

Incoming Data

↓

Partition Class-1 and outermost TE Symbols

↓

Symbols^4

↓

VVPE (Block Size N1)

$e^{-j\varphi_{est}}$ φ_{est}

⊗

↓

(c) CT

64-QAM — QPSK Transformation

↓

Symbols^4

↓

VVPE (Block Size N2)

φ_{QPSK}

⊗

$e^{-j\varphi_{QPSK}}$

↓

(d) MLE

ML Estimator (Block Size N3)

↓ φ_{ML}

⊗

$e^{-j\varphi_{ML}}$

↓

BER Decision

⋯

↓

ML Estimator (Block Size N4)

↓ φ_{ML}
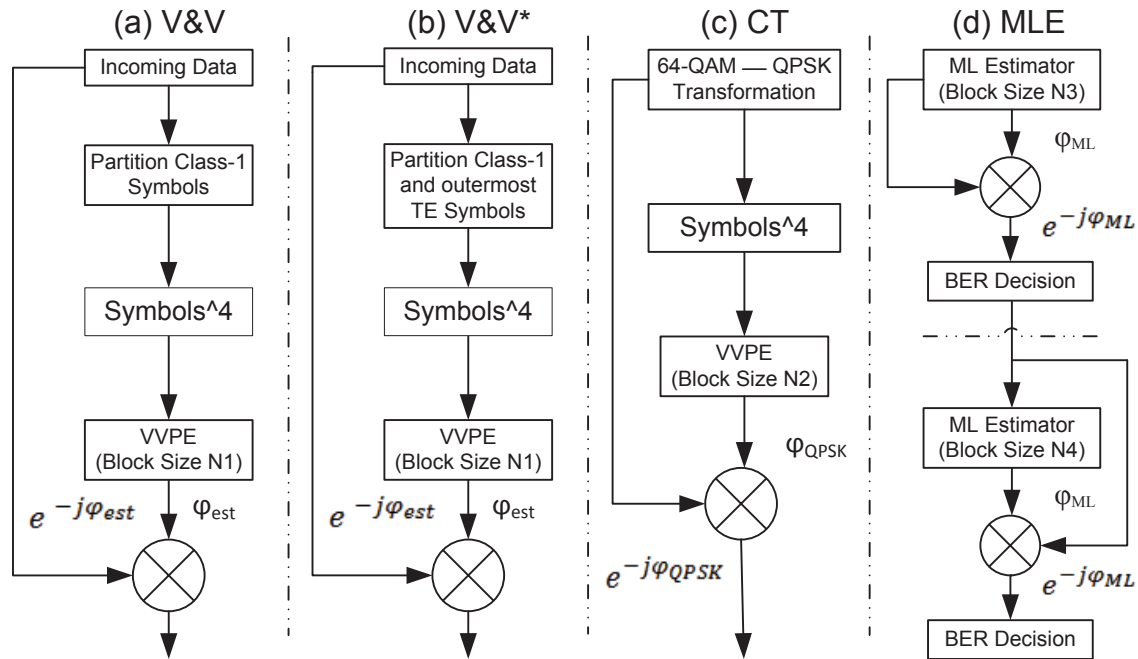
⊗

$e^{-j\varphi_{ML}}$

↓

BER Decision

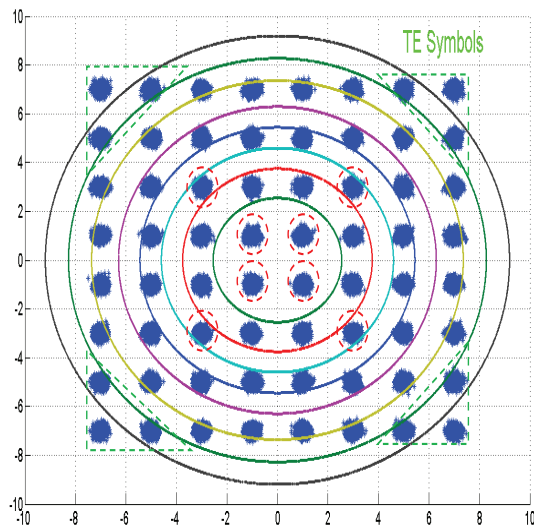Fig. 3. Block diagrams of the elementary CPE stages

Fig. 2. 64-QAM Constellation with different thresholds for separating symbols of different amplitudes. Symbols used in the first Viterbi&Viterbi stage are highlighted by red dashed circles & green triangles .

Fig. 4. 64-QAM constellation plot with class-1 symbols rotated by $\pi/8$ and approximately aligned with the Class-2 symbols

symbols, while using a uniform filter with centered window. Since the triangle edge symbols lie at an angle of $\pm 9.5°$ from $m \cdot \pi /4$ (m=1, 3, 5, 7), raising them to the power of 4 will approximately reduce them to the single phase vectors and if the averaging window is sufficiently long this $\pm 9.5°$ error is averaged out and the estimation of phase noise is only marginally affected by these errors.

In [21], we have presented an approach in which Class-1 symbols are rotated by $\pi /8$ so that they can be approximately aligned with the Class-2 symbols (symbols that lie an angle
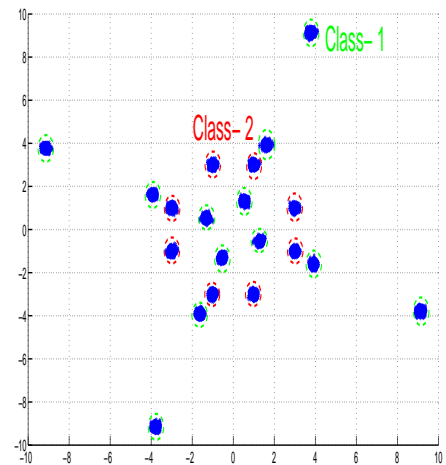
of $\pm \theta_{rot} = \pi /4$ - arctan(1/3) from Class-1 symbols). All the symbols are then raised to the power of 8 and the conventional V&V algorithm was applied afterwards (see Fig. 4) for CPE.

The technique presented here is somewhat similar to the one proposed in [21], but since the symbols are raised to the power of 4 instead of 8, the technique can be easily used for a higher target BER (10^{-2}).

IV. CONSTELLATION TRANSFORMATION (CT)

After getting a coarse estimate by applying the Viterbi&Viterbi algorithm to Class-1 symbols, a finer
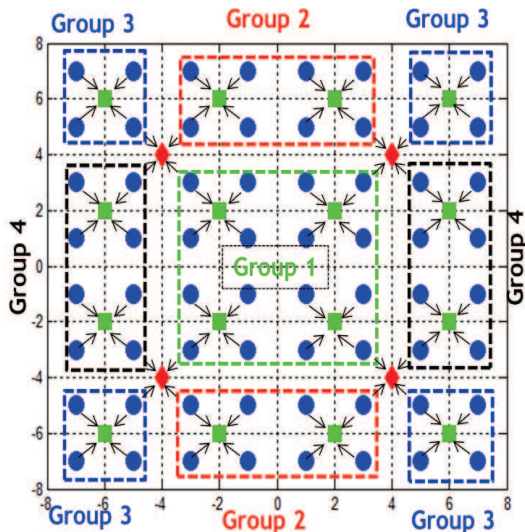
Fig. 5. 64-QAM to QPSK transformation

estimation can then be obtained by reducing the 64-QAM constellation down to QPSK.

For this purpose, 16-QAM pairing is done on a 64-QAM constellation (see Fig. 5). After an initial phase noise correction, it is possible to divide the 64-QAM constellation into four 16 QAM pairs, as shown in Fig. 5. In order to reduce the 64-QAM constellation down to 16-QAM, the following equation was used [17]:

$$X = Y_{1r} - sgn\left(Y_{1r} - 2sgn\left(Y_{1r}\right)\right) \qquad (4)$$

$$+j\left(Y_{1i} - sgn\left(Y_{1i} - 2sgn\left(Y_{1i}\right)\right)\right)$$

$$+Y_{2r} - sgn\left(Y_{2r} - 2sgn\left(Y_{2r}\right)\right)$$

$$+j\left(Y_{2i} - sgn\left(Y_{2i} - 6sgn\left(Y_{2i}\right)\right)\right)$$

$$+Y_{3r} - sgn\left(Y_{3r} - 6sgn\left(Y_{3r}\right)\right)$$

$$+j\left(Y_{3i} - sgn\left(Y_{3i} - 6sgn\left(Y_{3i}\right)\right)\right)$$

$$+Y_{4r} - sgn\left(Y_{4r} - 6sgn\left(Y_{4r}\right)\right)$$

$$+j\left(Y_{4i} - sgn\left(Y_{4i} - 2sgn\left(Y_{4i}\right)\right)\right)$$

where $Y_{1,[r\ i]}$, $Y_{2,[r\ i]}$, $Y_{3,[r\ i]}$ & $Y_{4,[r\ i]}$ are the real and imaginary parts of the four QPSK group pairs shown in Fig. 5 and $sgn(.)$ is the 'signum' function.

The symbols X of the obtained 16-QAM constellation are then further reduced to QPSK (Fig. 5) by using the mathematical equation [19]:

$$Z = X_r - 2sgn\left(X_r - 4sgn\left(X_r\right)\right) \qquad (5)$$

$$+j\left(X_i - 2sgn\left(X_i - 4sgn\left(X_i\right)\right)\right)$$

After this, all the symbols are raised to the power of four and the conventional VVPE algorithm is applied afterwards to obtain a fine estimate (see Fig. 3c). Again averaging is performed over N_2 symbols, while using a uniform filter with centered window.

In Fig. 5, the 64-QAM constellation is indicated by blue color circles whereas 16QAM and QPSK constellations are shown by green squares and red diamonds, respectively. Arrows in the figure show the transformation of 64-QAM to 16-QAM and ultimately to QPSK. It is important to note that this algorithm can only be used after frequency offset compensation between the local oscillator and transmitter laser and after an initial phase noise correction using a coarse estimate. It is for this reason that, 64-QAM–QPSK transformation serves as a 2nd stage for phase noise compensation.

V. MULTI-STAGE CPE SCHEMES

Several multi-stage CPE algorithms can be obtained by combining the elementary stages described in the previous sections and whose block diagrams are shown in Fig. 3. As an example, the V&V* scheme can be used in the first stage for a coarse phase estimation, which is then refined in a second stage based on the CT algorithm. Finally, a further improved estimation is obtained by introducing a 3rd stage based on the MLE algorithm with averaging performed over N_3 symbols using a uniform filter with centered window. In order to overcome the residual phase noise, another MLE stage can be introduced with averaging performed over N_4 symbols using a uniform filter with centered window.

Fig. 6 shows the evolution of the constellation plots after frequency-offset compensation (Fig. 6a) and after each stage of phase offset-estimation. Note that, since the first CPE stage is based on the M-th power algorithm (with $M{=}4$), the maximum tolerable residual frequency offset is in the range $[-R_s/2M, +R_s/2M]$, i.e. $\pm R_s/8$. The corresponding values of BER are shown in the figure caption. The SNR and $\Delta\nu \cdot T_s$ at which the plots of Fig. 6 have been obtained are 25 dB and 10^{-4}, respectively. Fig. 6b shows the constellation plot after 1st stage of coarse carrier phase estimation. In Fig. 6c, blue, green and red coloured constellation points indicate the transformation of 64-QAM to 16-QAM and finally to QPSK, respectively. After frequency offset compensation, residual frequency offset causes the rotation of 64-QAM constellation. After coarse carrier phase compensation, residual phase noise distorts the constellation. Using the 4th power algorithm after 64-QAM–QPSK transformation an estimation of residual phase noise can be obtained. Using this estimation, a phase correction is applied, yielding the constellation shown in Fig. 6d. Finally, performance of the proposed estimators can further be improved by adding one or more MLE stages (Figs. 6e and 6f).

Phase unwrapping is very important and is needed for all the proposed schemes. Since the arg(.) function gives the values between $-\pi$ and $+\pi$, so it is not possible to distinguish the angles that vary by integer multiples of 2π. Without phase unwrapping the output will be restricted between $-\pi/M$ and $+\pi/M$. Hence by introducing an integer multiple of $2\pi/M$, phase unwrapping assures that the phase difference magnitude between the neighboring symbols is always smaller than π/M [9].
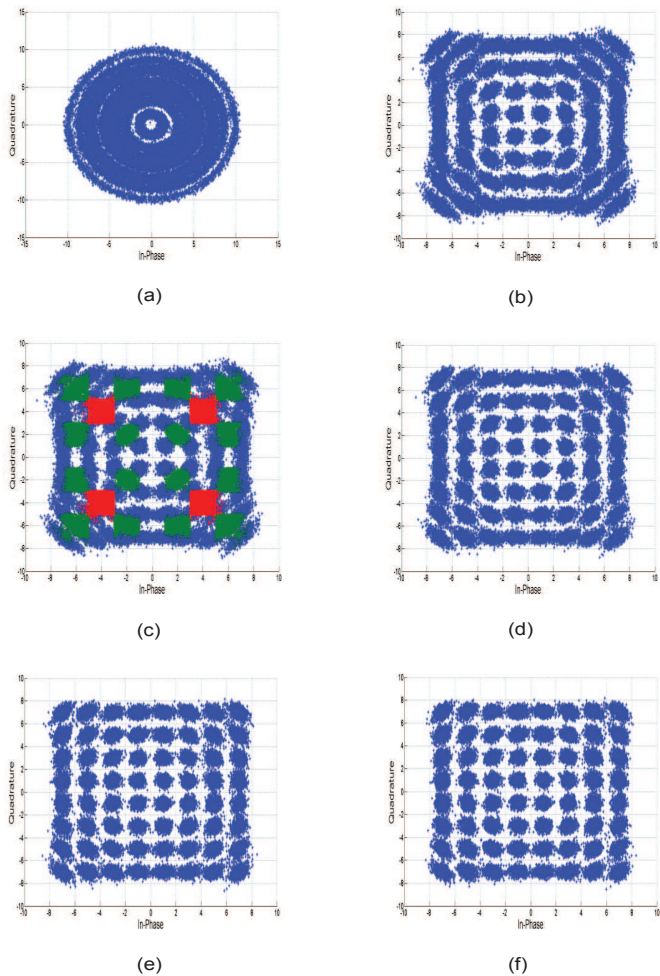
(a) (b)

(c) (d)

(e) (f)

Fig. 6. Constellation plot after : (a) frequency offset compensation (BER=4.6×10^{-1}) (b) 1st stage coarse estimate (BER=1.6×10^{-2}) (c) 64-QAM–QPSK Transformation (d) 2nd stage fine estimate using QPSK transform (BER=6×10^{-3}) (e) 3rd stage using MLE (BER=3.1×10^{-3}) (f) 4th stage using MLE (BER=2.0×10^{-3})
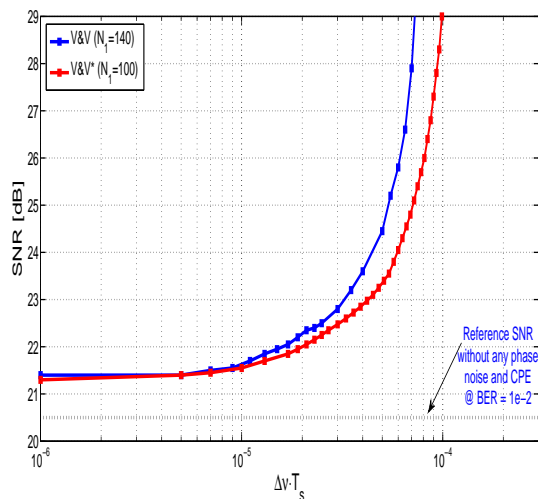

Fig. 7. A comparison of SNR vs linewidth times symbol duration ($\Delta \nu \cdot T_s$) for phase error estimate obtained by using only Class-1, and both Class-1+TE symbols
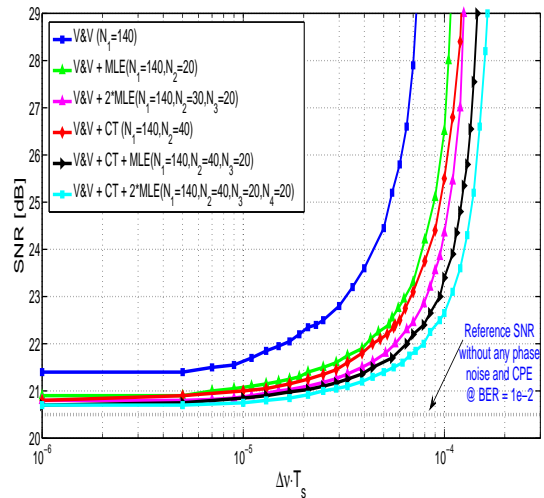

Fig. 8. SNR vs Linewidth times symbol duration ($\Delta \nu \cdot T_s$) for phase error estimate obtained by using only Class-1 symbols with subsequent stages
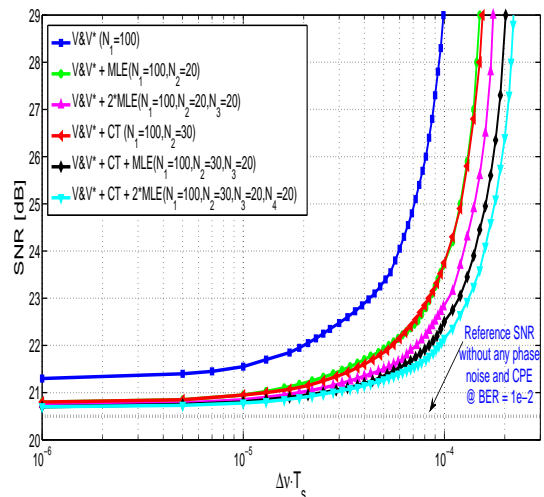

Fig. 9. SNR vs Linewidth times symbol duration ($\Delta \nu \cdot T_s$) for phase error estimate obtained by using only Class-1 + TE symbols with subsequent stages

VI. SIMULATION RESULTS AND DISCUSSION:

In this section we compare by simulation the performance of several multi-stage algorithms obtained by combining the elementary stages described in the previous sections. A total of 12 different algorithms are analyzed, whose composition in terms of elementary stages is shown in Table I.

The equalized signal samples, affected by both additive Gaussian noise and phase noise, can be written as:

$$y_k = x_k e^{j\theta_k} + n_k \qquad (6)$$

x_k is the data symbol that belongs to the set ($\pm a \pm j \cdot b$), a, $b \in \{1, 3, 5, 7\}$ and n_k is the additive white Gaussian noise (AWGN), which models for instance the ASE noise introduced by optical amplifiers. θ_k is the laser phase noise and is modeled as a Wiener process [14], as shown in Fig. 10.
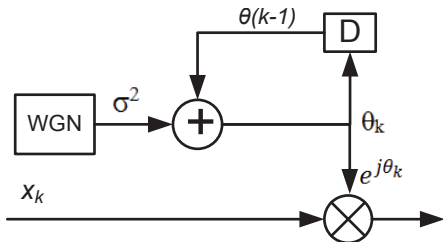
Fig. 10. Phase Noise Model

$$\theta_k = \sum_{i=-\infty}^{k} v_i \qquad (7)$$

v_i's are independent and identically distributed Gaussian random variables with zero mean and variance

$$\sigma_f^2 = 2\pi\Delta\nu \cdot T_s \qquad (8)$$

$\Delta\nu$ is the laser linewidth and T_s is the symbol period.

In our simulations, each 64-QAM symbol was generated combining 4 different PRBS sequences of length equal to $2^{15}-1$ and the BER was evaluated by error counting over ~100,000 symbols. Fig. 7 shows the performance comparison between the two single-stage algorithms using only Class-1 and Class-1 + TE symbols in terms of SNR (defined over a bandwidth equal to the symbol-rate $R_s = 1/T_s$) required to obtain a target BER equal to 10^{-2} as a function of the product $\Delta\nu \cdot T_s$. We chose the target BER so that the system can tolerate a 1dB SNR penalty due to phase noise without exceeding the FEC threshold, which is assumed to be 2×10^{-2}, as granted by current state-of-the-art soft FEC codes with 20% overhead [23]. No cycle slip was detected in our simulations. However, considering lower SNR values and larger line-widths, cycle slips could indeed occur, and could be compensated by using either differential encoding or the technique proposed in [22]. In fact, the techniques proposed in this paper do not have any particular effect in mitigating cycle slips.

Fig. 7 shows an example of the gain that can be achieved by increasing the number of constellation points used for carrier phase estimation: comparing the performance of V&V (which uses 12 points) with the one of V&V* (which uses 20 points), the latter has an optimum averaging window length of 100 symbols (vs. 140 symbols), with an increase in terms of linewidth tolerance at 1-dB penalty at BER=10^{-2} from 8×10^{-6} to 10^{-5}.

The value of the averaging window length which minimizes the BER depends on the value of the laser linewidth. A large value of the window length gives a good performance in the absence of phase noise, but does not give a good phase noise tolerance when the laser linewidth increases. In this study we chose the value of the averaging window length that maximizes the linewidth tolerance at 1-dB penalty, which we deemed to be a good compromise between a reasonable back to back performance and a good linewidth tolerance.

For a lower target BER of 10^{-3}, the algorithm using Class-1+TE symbols works almost the same as the one using only

1st Stage	2nd Stage	3rd Stage	4th Stage	LW Tolerance
V&V				8.0×10^{-6}
V&V*				1.0×10^{-5}
V&V	MLE			2.5×10^{-5}
V&V	MLE	MLE		3.9×10^{-5}
V&V*	MLE			3.7×10^{-5}
V&V*	MLE	MLE		5.3×10^{-5}
V&V	CT			3.0×10^{-5}
V&V*	CT			3.7×10^{-5}
V&V	CT	MLE		4.5×10^{-5}
V&V	CT	MLE	MLE	5.6×10^{-5}
V&V*	CT	MLE		6.0×10^{-5}
V&V*	CT	MLE	MLE	7.1×10^{-5}

TABLE I
LASER PHASE NOISE TOLERANCES

Class-1 symbols. This is because at lower target BER the error of ±9.5° is large enough to overcome the advantage of increase in the number of symbols for phase estimation decision and hence results in considerable degraded performance.

The linewidth tolerance can be improved by adding further CPE stages, as shown in Figs. 8 and 9. It can be observed that the proposed four-stage schemes, based on the 64-QAM–QPSK transformation, have a high phase noise tolerance: Table I shows the linewidth tolerances (i.e linewidth times symbol duration products) at 1-dB penalty with respect to the SNR needed to achieve BER=10^{-2} in the absence of phase noise (i.e. $\approx$ 20.5 dB). When using V&V as the first stage, the optimum (i.e. maximizing the linewidth tolerance at 1-dB penalty) values of the averaging window length for the second stage CT and the subsequent MLE stages were found to be around 40 (N_2=40) and 20 ([N_3 N_4]=20), respectively. When using the modified V&V* algorithm as the first stage, the averaging window length for the second stage CT and the subsequent MLE stages were found to be around 30 (N_2=30) and 20 ([N_3 N_4]=20), respectively.

The smaller value of the averaging window length for V&V* with respect to V&V is due to the fact that, for 64-QAM, V&V (with only Class-1 symbols) makes an estimate using only subset of Class-1 symbols i.e 19% of the total symbols whereas V&V* (with Class-1 + TE symbols) makes an estimation by using approximately 31% of the total symbols. A similar decrease in the averaging window length can be observed at the 2nd 64-QAM–QPSK CT stage which uses 40 symbols (N_2=40) for V&V and 30 symbols (N_2=30) for V&V*, respectively. Hence in comparison to V&V (with only Class-1 symbols), using V&V* (with Class-1 + TE symbols) at the 1st stage, a better $\Delta\nu \cdot T_s$ and optimum averaging window length can be obtained.

The two-stage algorithms with V&V (Class-1 or Class-1 + TE) + MLE or CT give very similar performance, while in the three-stage algorithms there is a little advantage in using CT + MLE with respect to two MLE blocks (see Fig. 8 and 9). This is likely due to the different decision strategy used in the two cases: while the MLE stage has to decide the exact symbol that has been transmitted, the CT block just need to

select the "region" in which the transmitted symbol falls (see [17] for details) and thus it is less affected by decision errors. The best performance is obtained when cascading 4 blocks (V&V* + CT + 2*MLE). We have also verified that adding a further MLE block does not yield any linewidth tolerance improvement, i.e. the corresponding performance curves will be perfectly overlapped with the ones having 2*MLE stage.

VII. CONCLUSION

In this paper, we have analyzed and compared the performance of several multi-stage phase noise tolerant feed forward carrier phase estimation algorithms for 64-QAM. The first stage employs either a simple QPSK partitiong algorithm using only Class-1 symbols or modified QPSK partitioning scheme utilizing both Class-1 and outer most TE symbols. The second stage uses a 64-QAM–QPSK transformation and the subsequent stages iterate a MLE algorithm for phase estimation. For the proposed four-stage techniques, a linewidth times symbol duration product ($\Delta\nu \cdot T_s$) equal to 5.6×10^{-5} and 7.1×10^{-5} is tolerated for 1-dB penalty at BER equal to 10^{-2}, respectively. Assuming the industry-standard symbol rate of 32 GBaud, this means that a total combined linewidth of over 1.7 MHz could be tolerated, making it possible to operate optical 64-QAM systems with current commercial tunable lasers. Note that the linewidth tolerance of the proposed algorithms is only slightly worse than the performance of the techniques based on the Blind Phase Search (BPS) [14], [24], which, at the reference BER of 10^{-2}, is around 8.0×10^{-5}, with a number of test phases B equal to 64 and an averaging window length N=20.

As for the complexity issue, we would like to point out that the real complexity strongly depends on the actual hardware implementation of the various algorithms, as shown in [14]. However, the complexity of BPS algorithm can be roughly estimated to be B times higher than the one of the V&V, CT and MLE algorithms [14], [24], when the same averaging window length is used. For 64QAM, B have to be at least equal to 64 to avoid losses in performance (see [14] and [24] for details). A rough estimation of the complexity reduction when using the 4-stage proposed algorithm, taking into account the optimum averaging window length reported in this paper, is of the order of a factor of 8 with respect to the standard BPS algorithm, and a factor of 2.5 with respect to the BPS/ML algorithm [24].

ACKNOWLEDGEMENTS

REFERENCES

[1] S. Zhang, P.-Y. Kam, C. Yu, and J. Chen, "Decision-aided carrier phase estimation for coherent optical communications," *Lightwave Technology, Journal of*, vol. 28, no. 11, pp. 1597 –1607, june1, 2010.

[2] A. Gnauck, P. Winzer, S. Chandrasekhar, X. Liu, B. Zhu, and D. Peckham, "10 x 224-Gb/s WDM transmission of 28-Gbaud PDM 16-QAM on a 50-GHz grid over 1,200 km of fiber," in *Proc. of OFC/NFOEC 2010, San Diego, paper PDPB8*, March 2010.

[3] K. Kikuchi, "Analyses of wavelength- and polarization-division multiplexed transmission characteristics of optical quadrature-amplitude-modulation signals," *Opt. Express*, vol. 19, no. 19, pp. 17 985–17 995, Sep 2011.

[4] X. Zhou and J. Yu, "200-Gb/s PDM-16QAM generation using a new synthesizing method," in *Proc. of ECOC 2009, Vienna (Austria), paper 10.3.5*, September 2009.

[5] A. Sano, T. Kobayashi, K. Ishihara, H. Masuda, S. Yamamoto, K. Mori, E. Yamazaki, E. Yoshida, Y. Miyamoto, T. Yamada, and H. Yamazaki, "240-Gb/s polarization-multiplexed 64-QAM modulation and blind detection using PLC-LN hybrid integrated modulator and digital coherent receiver," in *Proc. of ECOC 2009, Vienna (Austria), paper PD2.2*, September 2009.

[6] L. Kazovsky, "Impact of laser phase noise on optical heterodyne communication systems," *Journal of Optical Communications.*, vol. 7, no. 2, pp. 41–80, june 1986.

[7] ——, "Performance analysis and laser linewidth requirements for optical PSK heterodyne communications systems," vol. 4, no. 4, apr 1986, pp. 415 – 425.

[8] A. Tarighat, R. Hsu, A. Sayed, and B. Jalali, "Digital adaptive phase noise reduction in coherent optical links," *Lightwave Technology, Journal of*, vol. 24, no. 3, pp. 1269 –1276, march 2006.

[9] E. Ip and J. M. Kahn, "Feedforward carrier recovery for coherent optical communications," *J. Lightwave Technol.*, vol. 25, no. 9, pp. 2675–2692, Sep 2007.

[10] H. Louchet, K. Kuzmin, and A. Richter, "Improved DSP algorithms for coherent 16-QAM transmission," in *Proc. of ECOC 2008, Brussels (Belgium), paper Tu.1.E.6*, September 2008.

[11] I. Fatadin, D. Ives, and S. J. Savory, "Blind equalization and carrier phase recovery in a 16-QAM optical coherent system," *J. Lightwave Technol.*, vol. 27, no. 15, pp. 3042–3049, Aug 2009.

[12] Y. Mori, C. Zhang, K. Igarashi, K. Katoh, and K. Kikuchi, "Unrepeated 200-km transmission of 40-Gbit/s 16-QAM signals using digital coherent receiver," *Opt. Express*, vol. 17, no. 3, pp. 1435–1441, Feb 2009.

[13] Y. Gao, A. Lau, C. Lu, J. Wu, Y. Li, K. Xu, W. Li, and J. Lin, "Low-complexity two-stage carrier phase estimation for 16-QAM systems using QPSK partitioning and maximum likelihood detection," in *Proc. of OFC/NFOEC 2011, Los Angeles, paper OMJ6*, March 2011.

[14] T. Pfau, S. Hoffmann, and R. Noe, "Hardware-efficient coherent digital receiver concept with feedforward carrier recovery for M-QAM constellations," *Lightwave Technology, Journal of*, vol. 27, no. 8, pp. 989 –999, april15, 2009.

[15] M. Seimetz, "Laser linewidth limitations for optical systems with high-order modulation employing feed forward digital carrier phase estimation," in *Proc. of OFC/NFOEC 2008, San Diego, paper OTuM2*, Feb. 2008.

[16] I. Fatadin, D. Ives, and S. Savory, "Laser linewidth tolerance for 16-QAM coherent optical systems using QPSK partitioning," *Photonics Technology Letters, IEEE*, vol. 22, no. 9, pp. 631 –633, may1, 2010.

[17] S. M. Bilal, G. Bosco., P. Poggiolini, and C. Fludger, "Low-complexity linewidth-tolerant carrier phase estimation for 64-QAM systems based on constellation transformation," in *Proc. of ECOC 2013, London (United Kingdom), paper P.3.7*, September 2013.

[18] S. M. Bilal and G. Bosco, "Dual stage carrier phase estimation for 16-QAM systems based on a modified QPSK-partitioning algorithm," in *Proc. of ICTON 2013, Cartagena (Spain), paper We.D1.2*, June 2013.

[19] J. H. Ke, K. P. Zhong, Y. Gao, J. Cartledge, A. Karar, and M. Rezania, "Linewidth-tolerant and low-complexity two-stage carrier phase estimation for dual-polarization 16-QAM coherent optical fiber communications," *Lightwave Technology, Journal of*, vol. 30, no. 24, pp. 3987–3992, 2012.

[20] S. M. Bilal, C. Fludger, and G. Bosco., "Multi-stage CPE algorithms for 64-QAM constellations," in *Proc. of OFC/NFOEC 2014, San Francisco, paper M2A.8*, March 2014.

[21] S. M. Bilal, A. Carena, C. Fludger, and G. Bosco., "Dual stage CPE for 64-QAM optical systems based on a modified QPSK-partitioning algorithm," *Photonics Technology Letters, IEEE*, vol. 26, no. 3, pp. 267–270, february 1, 2014.

[22] Y. Gao, A. Lau, C. Lu, Y. Dai, and X. Xu, "Blind cycle-slip detection and correction for coherent communication systems," in *Proc. of ECOC 2013, London (United Kingdom), paper P.3.16*, September 2013.

[23] Y. Miyata, K. Sugihara, W. Matsumoto, K. Onohara, T. Sugihara, K. Kubo, H. Yoshida, and T. Mizuochi, "A triple-concatenated FEC using soft-decision decoding for 100 Gb/s optical transmission," in *Proc. of OFC/NFOEC 2010, San Diego, paper OThL3*, March 2010.

[24] X. Zhou, "An improved feed-forward carrier recovery algorithm for coherent receivers with M -QAM modulation format," *Photonics Technology Letters, IEEE*, vol. 22, no. 14, pp. 1051–1053, July 2010.